State Feedback Control of an Underwater Vehicle for Wall Following

D. Maalouf, V. Creuze, and A. Chemori

***Abstract*—Wall following consists in navigating at a constant distance and orientation from a certain surface to be inspected. This task is required in many applications of underwater vehicles (e.g. ship hull or hydraulic dam inspection). We propose a nonlinear state feedback, designed for a specific embedded acoustic sensing system. The proposed method and the associated sensor can work on very small low cost underwater vehicles at high sampling rates. Sensor experiments show the ability of a single beam transducer to detect both distance and orientation of a wall, while simulation results show how this sensing system can be successfully integrated in a nonlinear state feedback controller to perform autonomous wall following with an underwater vehicle, even with disturbances.**

I. Introduction

UNDERWATER robotic vehicles have known an impressive increase of their field of application. They are now able to achieve various tasks with an increased level of autonomy. After two decades of development, Autonomous Underwater Vehicles (AUV) have reached a good industrial stage [1][2]. Remotely Operated Vehicles (ROVs) are acquiring new capabilities to assist the pilot. In order to allow the pilot to focus on the main aspects of the mission, a part of his usually dedicated tasks such as hovering [3], station keeping [4], ship hull following [5] becomes autonomous. One of the applications of underwater vehicles (ROVs or AUVs) is wall inspection. It consists in navigating at a constant distance from a wall (e.g. hydraulic dam, cf. Fig. 1) to monitor the state of the inspected structure (crack detection) [6]. During the mission, the vehicle performs video or sonar imaging. The ship hull inspection is similar and is performed to detect mines or weaknesses. Using underwater vehicles avoids the use of a dry berth and inspection can be conducted at sea. Automation of wall/hull following can be used either to assist the ROV's pilot or to perform full automatic inspection with an AUV. However, performing automatic wall or ship hull inspection requires resolving two problems, namely guidance/control and positioning:

- Guidance/control consists in computing a desired state and the associated control law such that the vehicle navigates at a constant distance from the inspected surface and keeps a constant orientation with respect to this surface (i.e. constant orientation relative to the inspected surface to enhance the quality of video or sonar imaging).
- Positioning consists in estimating the vehicle position relative to the inspected structure in order to retrieve the location of any observed anomalies.

Positioning is a difficult task, made harder by the very disturbed magnetic environment and by the fact that the surface is mainly flat (no visual landmarks) or slowly moving (hull inspection of a moored ship). The video can be used to estimate the vehicle's position in cases where the surface is irregular enough (asperities, algae, etc.)[7], while on very regular surfaces it is required to use Doppler Velocity Log (DVL) as does Bluefin HAUV [5]. Positioning problem is beyond the scope of this paper, however a very interesting work about this topic can be found in [5] and [7].

This paper will focus on distance and orientation servoing of an underwater vehicle achieving wall following. Two main contributions are proposed in this paper:

- A new acoustic sensing system relying on processing of the echo obtained by a single transducer, and allowing finding out both distance and orientation of the wall.
- Association of this sensor with a controller allowing constant distance/orientation wall following.

This paper is organized as follows. In section II, the problem statement is introduced. The principles of our acoustic sensor and the signal processing scheme used to compute distance and orientation of the inspected surface are presented in section III. Section IV is devoted to the proposed control approach, and section V presents the obtained results (experiments and simulations). The paper ends with some concluding remarks.

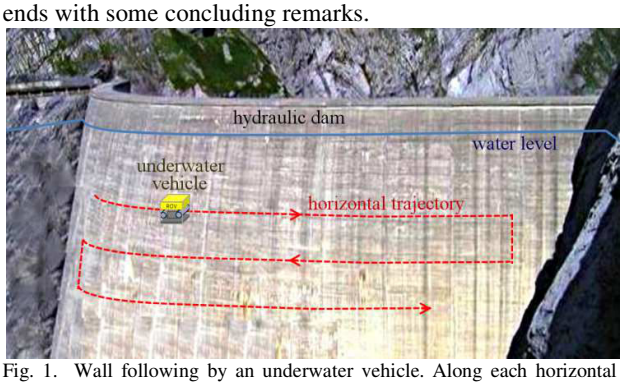

Fig. 1. Wall following by an underwater vehicle. Along each horizontal trajectory, the vehicle navigates at constant depth, at a constant distance from the wall, and with a constant orientation relative to the wall surface.

D. Maalouf is with the LIRMM, University Montpellier 2 / CNRS , UMR5506, CC477, 161 rue Ada, 34095 Montpellier Cedex 5, FRANCE (phone: +33.467.418.514; fax: +33.467.418.500; e-mail: divine.maalouf@lirmm.fr).

V. Creuze and A. Chemori are with the LIRMM (e-mail: vincent.creuze@lirmm.fr, ahmed.chemori@lirmm.fr).

II. Problem Statement

A. Problem Statement

Let us consider an underwater vehicle aiming to follow a wall horizontally (i.e. at a constant depth), at a constant distance ($1\,m$) and with a constant orientation with respect to the wall (cf. Fig. 1). As mentioned above, positioning is not considered in this paper since it is treated separately by fusing video and acoustic data. The main topic of this paper is the **association of the perception system to the proposed controller.**

B. Guidance

Guidance consists in continuously computing the desired position, velocity or acceleration. To detect distance and orientation of the wall, several schemes have been proposed in the literature. One can either use sonar [6] but this high cost technique (more than 5k$) suffers from low sampling rate and high bandwidth emission, which increases significantly the risk of interference with other acoustic devices (e.g. modem). One can also use video associated with laser triangulation as successfully demonstrated by Caccia [3], but the efficiency of optical methods decreases when water turbidity increases.

Another technique consists in using the four range measurements of an acoustic Doppler Velocity Log (DVL) as experimented with the Bluefin HAUV [5]. This technique avoids the drawbacks of the two previous ones (sampling rate, water turbidity), but it remains expensive (more than 10k$) in comparison with the price of a very small ROV (e.g. VideoRay, Seabotix, AC-ROV, etc.). In the case of [5], the use of the DVL is justified by the fact that DVL is also used to estimate position. Moreover, as with sector scanning sonar (sizing at least 10cm x 6cm²), DVL sensor is quite big to be associated to a small underwater vehicles. In fact, it would require more powerful thrusters, and would also reduce the payload.

In our case, a simple single beam acoustic transducer is used with the detection method introduced in [8] and improved in [11]. Although it requires only a single beam transducer, signal processing allows finding out not only distance but also orientation of the target. In comparison with other acoustic methods, ours offers the highest sampling rate (only one ping is required to compute both distance and orientation) and shortest acquisition time (in comparison with sector scanning sonar for instance). Moreover, the single frequency emission minimizes interferences possibility with other acoustic devices (e.g. modem). The sensor is also basic, cheap and small (in comparison with arrays of sensors), with low power consumption and computational cost, thus allowing its use on very small autonomous vehicles. The principle of this sensing method will be briefly introduced in section III.

C. Control

The control is done in conjunction with the guidance and consists in determining the control forces and torques to be applied to follow a desired position, velocity, and acceleration. We propose a nonlinear state feedback controller adapted to the presented sensing method. This controller is detailed in section IV.

III. Acoustic Sensing

A. Directivity Pattern

The directivity pattern $b(\theta)$ of a disc-shaped transducer is given by:

$$b(\theta) = \left(\frac{2J_1\left(2\pi f \frac{r_c}{c} \sin\theta\right)}{2\pi f \frac{r_c}{c} \sin\theta} \right)^2 \quad (1)$$

where $J_1(.)$ is the first order Bessel function, f is the acoustic wave frequency ($200\,kHz$), r_c is the transducer radius, and c is sound speed in water ($1500\,m.s^{-1}$) [9]. A polar representation of the beam pattern in decibels highlights the main lobe and sidelobes (cf. Fig. 2). In the following, "sidelobe" will denote only the first sidelobe (the other sidelobes are weak enough to be neglected).

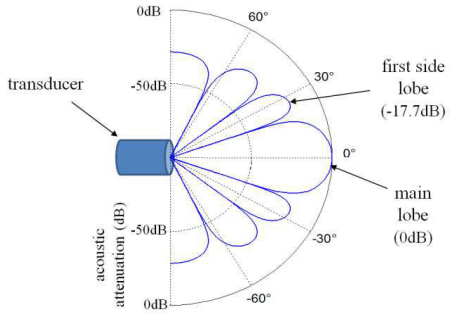

Fig. 2. Directivity pattern of a disc shaped transducer (radius=13.5 mm, *f*=200 kHz). The first sidelobe attenuation is -17.7dB.

B. Wall Surface Backscattering

Sound emitted by the transducer will be partially backscattered by the wall. The target strength TS is given by [9]:

$$TS = S_s + 10\log A \quad (2)$$

where S_s denotes the backscattering strength of the wall, and A denotes the extent of the wall area which contributes to the backscattered signal.

For incidence angle φ_i beyond *25°*, a good approximation of the backscattering strength S_S is given by following Lambert's law [10]:

$$S_S = S_0 + 10\log\cos^2\varphi_i \quad (3)$$

where S_0 is a constant parameter depending on the wall characteristics, and φ_i is the incidence angle.

For incidence angles φ_i less than 25°, the backscattering strength S_S can be approximated by (linear approximation):

$$S_S = S_N + \frac{\varphi_i}{\varphi_0}(S_0 - S_N + 10\log\cos^2\varphi_0) \quad (4)$$

where S_N is the backscattering strength for normal incidence and φ_0 is called the transition direction.

C. Distance and Orientation of the Wall

The sidelobe has usually no effect and can be neglected. However, if the transducer is tilted enough, the incidence

angle of the main lobe becomes larger than that of the sidelobe. Therefore, the backscattering strength is smaller for the main lobe signal than for the sidelobe. Moreover, due to the difference in length of the sound paths, transmission losses TL (mainly spherical spreading, as the distance is short) are smaller for the sidelobe than for the main lobe. Consequently, in spite of directivity attenuation, the global attenuation level makes the sidelobe echo level significant in comparison with the main lobe echo level. Then the backscattered acoustic echo consists of two separated parts corresponding first to the sidelobe and secondly to the main lobe (cf. Fig. 3). We have proved [11] that ψ_s the orientation of the wall can be computed by measuring t_s and t_m, respectively the times of occurrence of the maxima of the two parts of the received echo, and solving equation (5).

$$t_s \cos(\psi_s - \gamma + \theta_s) - t_m \cos\big(\gamma - \psi_s + \hat{g}(\psi_s)\big) = 0 \quad (5)$$

where θ_s is the angle between the axis of the sidelobe and the axis of the main lobe, $\hat{g}$ is a second order polynomial obtained by calibration of the sensor, and γ is the tilt angle (assumed to be constant and known) of the transducer regarding the vehicle axis u.

Then d, the distance of the wall, can be computed as:

$$d = \frac{c.t_s/_2}{\sin\left(\frac{\pi}{2} + \psi_s\right)} \sin\left(\frac{\pi}{2} - \psi_s + \gamma - \theta_s\right) \quad (6)$$

The automatic peaks detection and distance/orientation computation is performed online with the algorithm detailed in [11]. It is worth to be mentioned that, due to the geometry of the first sidelobe (all around the main lobe), the inspected surface must be locally plane. As this latter is very large with respect to the beam, this assumption is almost always satisfied.

IV. Control

A. Dynamic Modeling of the Vehicle and Previous Work

The underwater vehicle is described by the six degrees of freedom vectorial SNAME model representation [12]:

$$\dot{\boldsymbol{\eta}} = \boldsymbol{J}(\boldsymbol{\eta})\boldsymbol{\nu}$$
$$\mathbf{M}\dot{\boldsymbol{\nu}} + \mathbf{C}(\boldsymbol{\nu})\boldsymbol{\nu} + \mathbf{D}(\boldsymbol{\nu})\boldsymbol{\nu} + \mathbf{g}(\boldsymbol{\eta}) = \boldsymbol{\tau} + \boldsymbol{w} \quad (7)$$

where

$$\boldsymbol{\nu} = [u, v, w, p, q, r]^T$$
$$\boldsymbol{\eta} = [x, y, z, \varphi, \theta, \psi]^T$$

are respectively vectors of velocities (in the body-fixed frame) and position/Euler angles (in the earth-fixed frame) (cf. Fig. 4), $\boldsymbol{J}(\boldsymbol{\eta}) \in \mathbb{R}^{6\times6}$ is the Euler angle transformation matrix. The model matrices **M**, **C** and **D** denote inertia (including added mass), Coriolis-centripetal (including added mass) and damping, respectively. **g** is a vector of gravitational/buoyancy forces and torques, $\boldsymbol{\tau}$ is the vector of control inputs (forces/torques) and $\boldsymbol{w}$ is the vector of external disturbances (waves and currents). The Euler angles representation has been chosen (instead of quaternion), as in our case maneuvers will always be far from the singular point $\theta = \pm 90°$.

We will consider the case of a ROV-type underwater vehicle. The control forces are assumed to be produced by four thrusters in fixed directions (i.e. nonrotatable), such that $\boldsymbol{\tau} = \boldsymbol{TKu}$, where $\boldsymbol{u}$ is the vector of control inputs, $\boldsymbol{K}$ is the diagonal force coefficient matrix, and $\boldsymbol{T}$ is the actuators configuration matrix.

Several control strategies have been developed for applications such as bottom hovering [3,4] or wall/ship hull following [5,6]. For instance, the horizontal motion of the Romeo ROV [13] uses a PI gain scheduling controller able to reduce the robot dynamics to a nominal characteristic equation. Depending on applications, the control strategy has to be adapted to the sensing systems. For example, the ship hull inspection dedicated AUV designed by MIT Sea Grant AUV Lab and Bluefin Robotics uses an inner-outer loop controller [5]. The DVL and depth sensor provide setpoints for higher bandwidth inner loop, while low level controller uses an Inertial Measurement Unit (IMU). In such designs, the outer-loop bandwidth must be at least 3-5 times slower than the inner loop [5]. In our case, we have designed a nonlinear state feedback controller (cf. section IV.C) inspired by [12]. In this controller, a simplified dynamic model (presented in section IV.B) is used. The controller does not require the measurement of the full state of the vehicle but only a set of variables as illustrated in Fig. 5.

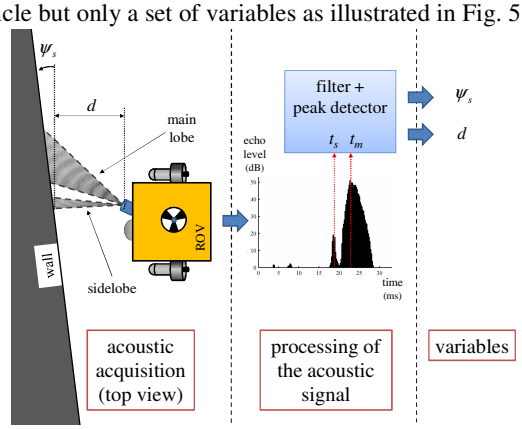

Fig. 3. The acoustic beam of a transducer with a circular aperture presents two lobes. When oriented such that the first sidelobe hits the target almost perpendicularly, its echo arrives first followed by the one of the main lobe. Computing the occurrence times of the peaks corresponding to sidelobe and main lobe allows finding out orientation and distance of the target (wall).

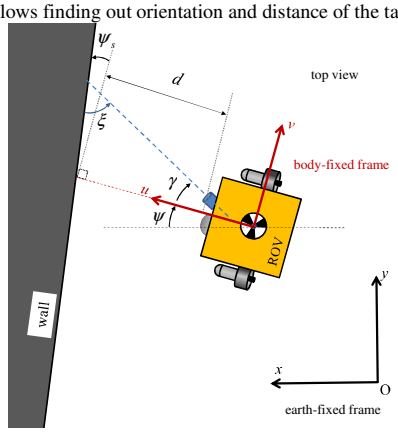

Fig. 4. The underwater vehicle (ROV type), its body-fixed frame (O,*u,v,w*), and the earth-fixed frame (O,*x,y,z*). *w* and *z* axes are oriented downwards. The ROV must keep distance *d* constant and must have a constant sway speed ($v = 0.3\ m.s^{-1}$). The *u* axis has to be maintained perpendicular to the wall surface (i.e. $\psi_s = 0$).

B. Nonlinear Dynamic Equation used in the Controller

Our vehicle is highly metacentric stable. That means gravitational and buoyancy centers are distant enough to ensure that the roll and pitch angles (φ, θ) are kept very small. These degrees of freedom will be left uncontrolled and assumed to be $\varphi \approx 0$ and $\theta \approx 0$. Consequently, for control purposes, a new velocity vector $\boldsymbol{\nu_2} = [u, v, w, r]^T$ is defined. Since the vehicle will move slowly (linear velocity about *0.3m.s*$^{-1}$), Coriolis matrix will also be neglected in the model used to design the controller and we will consider the following simplified dynamics equation:

$$\mathbf{M}\dot{\boldsymbol{\nu}}_2 + \mathbf{D}(\boldsymbol{\nu_2})\boldsymbol{\nu_2} + \mathbf{g_2} = \boldsymbol{\tau_2} \quad (8)$$

where $\boldsymbol{\tau_2}$ is the control forces vector, $\mathbf{M}$ and $\mathbf{D}(\boldsymbol{\nu_2})$ are obtained by simplifying the corresponding matrix in (7), and $\mathbf{g_2}$ is a constant vector $\mathbf{g_2} = [0,0,B-W,0]^T$, where B denotes the buoyancy and W the weight of the ROV.

The control forces/torques vector $\boldsymbol{\tau}$ of the full model defined in (7) is obtained from $\boldsymbol{\tau_2}$ as follows:

$$\boldsymbol{\tau} = \boldsymbol{H}\boldsymbol{\tau_2} \quad \text{with} \quad \boldsymbol{H} = \begin{bmatrix} 1 & 0 & 0 & 0 \\ 0 & 1 & 0 & 0 \\ 0 & 0 & 1 & 0 \\ 0 & 0 & 0 & 0 \\ 0 & 0 & 0 & 0 \\ 0 & 0 & 0 & 1 \end{bmatrix} \quad (9)$$

Since $\varphi \approx 0$ and $\theta \approx 0$, it is worth to be noted that $\mathrm{r} = \dot{\psi}$.

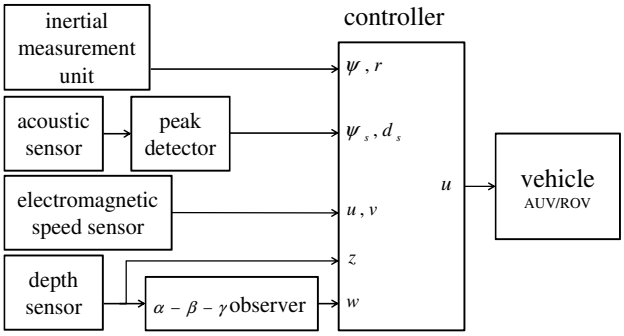

Fig. 5. Perception and control architecture of the underwater vehicle. The controller is based on state feedback linearization.

C. Nonlinear State Feedback Controller

State feedback linearization allows transformation of nonlinear systems' dynamics into a linear system [14] by compensating all the nonlinearities. Consider the following control law:

$$\boldsymbol{\tau_2} = \boldsymbol{M}\boldsymbol{a^b} + \mathbf{D}(\boldsymbol{\nu_2})\boldsymbol{\nu_2} + \mathbf{g_2} \quad (10)$$

where $\boldsymbol{a^b}$ is the body-fixed desired acceleration vector.
(10) replaced in (8) leads to the following closed-loop linearized dynamics of the vehicle:

$$\dot{\boldsymbol{\nu}}_2 = \boldsymbol{a^b} \quad (11)$$

Then $\boldsymbol{a^b}$ is chosen as a PI-controller with feedback acceleration:

$$\boldsymbol{a^b} = \dot{\boldsymbol{\nu}}_{2d} - 2\boldsymbol{\Lambda}\tilde{\boldsymbol{\nu}}_2 - \boldsymbol{\Lambda}^2 \int_0^t \tilde{\boldsymbol{\nu}}_2(\tau)d\tau \quad (12)$$

where $\boldsymbol{\Lambda} = \mathrm{diag}\{\lambda_1, \lambda_2, \lambda_3, \lambda_4\}$ allows to chose the desired poles of the desired closed-loop dynamics, $\dot{\boldsymbol{\nu}}_{2d}$ is the desired value of $\dot{\boldsymbol{\nu}}_2$, and $\tilde{\boldsymbol{\nu}}_2 = \boldsymbol{\nu_2} - \boldsymbol{\nu_{2d}}$ is the velocity tracking error.

Assuming that the wall varies very slowly (i.e. small geometric variations) in comparison with the moving of the vehicle, it can be seen from Fig. 4 that :

$$u_d \approx \dot{d}_s \quad \text{and} \quad r_d = \dot{\psi}_d \quad (13)$$

where ψ_d is the desired yaw angle, defined by $\psi_d = \psi_v - \psi - \pi/2$, where ψ_v is the current yaw angle of the vehicle and ψ is the wall angle measured by the acoustic sensor.

Considering that we want to keep constant the values of $v_d = 0.3\ m.s^{-1}$ and $z_d = 5\ m$, therefore $\dot{v}_d = 0\ m.s^{-2}$, $w_d = 0\ m.s^{-1}$, and $\dot{w}_d = 0\ m.s^{-2}$.

Before being used in the control law, all the desired signals are filtered with second order reference models, whose parameters (ζ, ω_0) have been chosen to respect the dynamics capabilities of the vehicle [12].

V. RESULTS

A. Sensor Experiments

We have performed pool tests of the above described acoustic sensing method applied to a disc-shaped transducer. Figure 5 shows an experimental acoustic acquisition made with the sensor under the following conditions: $d = 2.2m$, $\psi = +5°$. The values obtained by computing the time of arrival of the two peaks are $d = 2.18m$, and $\psi = +4.9°$. The range of orientation measurement is [-10° ; +10°], with an error smaller than 1°. The precision can be quantified by the distance error, which is smaller than 2% (range < 10m).

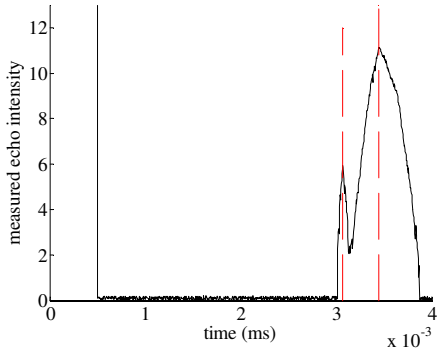

Figure 5 – Experimental acquisition of an acoustic echo (in a pool). Peaks can easily be detected and lead to an appropriate estimate of distance and orientation of the wall of the pool.

B. Numerical Simulation of the Proposed Controller

The proposed control approach has been simulated using the Marine System Simulator (MSS, version 3.3) [15] Matlab/Simulink© library developed at the Norwegian University of Science and Technology (NTNU) since 1991 by T.I. Fossen and T. Perez. The simulation has been carried out with ode45 solver (Dormand-Prince).

The full model described in (7) was used to compute the "true" state of the vehicle (position, orientation, linear and rotational speeds). However the controller is based on the simplified model (10) and applied to the "true" vehicle full

model. All the sensors (acoustic, IMU, depth, etc.), including measurement noise, have been modeled and their data were simulated from the "true" state of the vehicle and its position in the environment. The constraints of saturation on thrusters have been taken into account in the simulator.

The vehicle is controlled to follow a wall at a distance of $d_d = 1\ m$, at a constant depth $z_d = 5\ m$, keeping its body-fixed u-axis perpendicular to the wall surface and moving at a constant sway speed $v_d = 0.3\ m.s^{-1}$.

The shape of the wall is defined by the following equation $y(x) = 5\sin(\frac{\pi}{50}x)$, where x and y denote the coordinate in the earth-fixed frame (Fig. 4). The initial state of the ROV is described by vectors $\boldsymbol{\eta}(0) = [4,4,0.5,0,0,-0.1]^T$ and $\boldsymbol{\nu}(0) = [0,0,0,0,0,0]^T$.

Three simulation scenarios were implemented. The first one deals with wall following without external disturbances, however in the second one an external disturbances is considered, and in the last scenario modeling uncertainties are considered.

C. Scenario 1: Wall Following without External Disturbance

First we have tested the proposed controller without external disturbances, with perfect knowledge of the dynamic parameters of the vehicle. The only introduced uncertainties were the measurement noises. As the controller needs the derivative of several variables, sensors data are filtered (second order low-pass filter) before being used in the controller. The obtained simulation results are given in Fig.6 and Fig. 7. They show the effectiveness of the proposed control approach in terms of ability of the vehicle to follow the wall. The depicted curves show the evolution of the controlled variables, namely ψ_s, $d_s - d_d$, z, v and the corresponding (x, y) trajectory.

D. Scenario 2: Wall Following with External Disturbances

We have simulated effects induced by two types of disturbances: waves and sea currents.

1) Waves disturbance

Waves at the surface of the water lead to depth measurement disturbances. However, the bandwidth of these disturbances is most of time higher than the dynamic capabilities of the vehicle. We have filtered (Butterworth second order filter) the data measured by the pressure sensor (i.e. depth measurement), to reject disturbances whose frequency was higher than the dynamic bandwidth of the vehicle. The obtained result is depicted on figure 8, where it can be clearly seen that high frequency waves are rejected, and only low frequency waves (0.16Hz in this case) disturb depth control (desired depth is 5 meters). However, the effects of such waves can be treated by observer-based techniques, as described in [12].

2) Current disturbance

The effect of an irrotational stationary sea current has also been considered, and the obtained result for this simulation case study is represented by Fig. 9. From which, it can be clearly observed that the time required to reach the desired trajectory is increased with respect to the case without current disturbance (see Fig. 7). However, once the desired trajectory is reached, the vehicle remains on it as long as the sum of current and desired speed remains under the thrusters' capabilities.

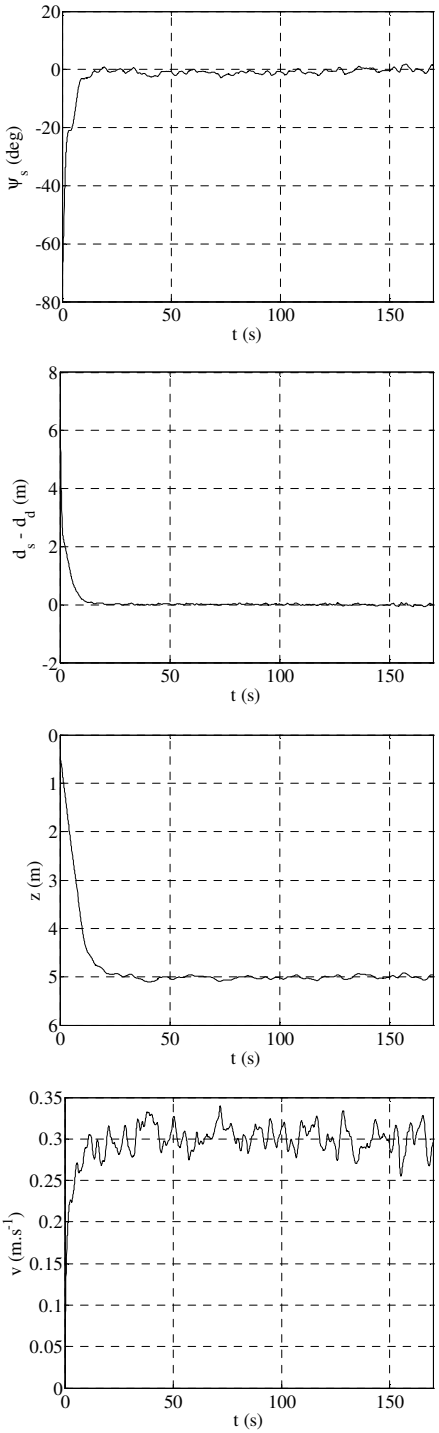

Fig. 6. Simulation results without disturbances. The measured wall orientation ψ_s relative to v-axis of the vehicle converges to 0°. The distance error $d - d_d$ measured between the wall and the vehicle also converges to 0°. Depth and sway speed converge to the desired values $z_d = 5\ m$ and $v = 0.3m.s^{-1}$.

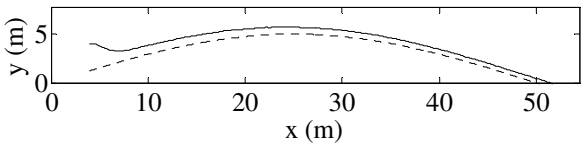

Fig. 7. Simulation results (without disturbances): the trajectory of the vehicle (solid line) and the wall (dashed line).

E. Scenario 3: Wall Following with Modeling Uncertainties

To evaluate the controller's robustness towards modeling uncertainties, we have considered uncertainties on some damping and inertial parameters of the vehicle.

For uncertainties on the damping matrix parameters smaller than 200%, the effect on the vehicle behavior is negligible. However, for larger uncertainties on these parameters, disturbances (mainly oscillations) occur on all the variables (including the degrees of freedom where no uncertainties have been considered).

We have also observed that the inertial parameter I_{zz} along the *w* axis of the body-fixed frame has an effect only on yaw servoing, what was not surprising. Indeed, with I_{zz} value two times smaller than the true one, we can see on Fig. 10 that ψ slowly oscillates (amplitude 5°).

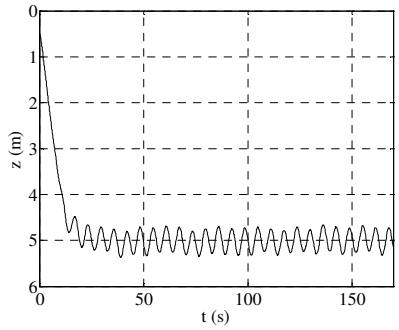

Fig. 8. The depth control can be affected by very low frequency waves.

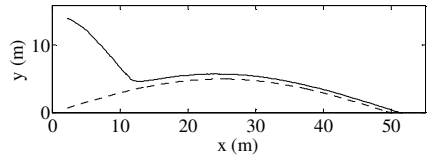

Fig. 9. It will take a longer time to reach the desired trajectory in presence of current when this latter leads to saturation of thrusters.

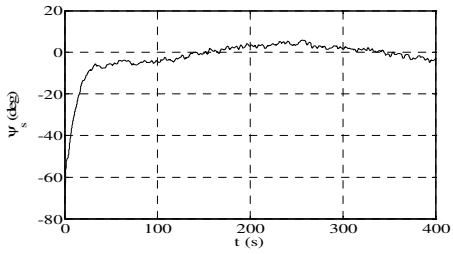

Fig. 10. The wall orientation ψ_s oscillates around the desired value (= 0 °) due to a -50% error on inertial parameter I_{zz}.

VI. Conclusion and Future Work

In this paper, we have presented a controller designed to guide an underwater vehicle to perform a wall following. The proposed controller is a nonlinear state-feedback based on a simplified dynamic model specially dedicated to this application. It takes into account the specificity of the presented acoustic sensing system. Experiments of this sensor have been presented, and simulation results have demonstrated a good ability of the vehicle to perform wall following. However, disturbances occur usually when some parameters are misestimated. Even if the proposed controller is able to compensate most of these disturbances, we are currently implementing and testing an adaptive nonlinear feedback controller in order to deal with strong uncertainties on parameters.

References

[1] R. P. Stokey, C. von Alt, B. Allen, N. Forrester, T. Austin, R. Goldsborough, M. Purcell, F. Jaffre, G. Packard, and A. Kukulya, "Development of the REMUS 600 Autonomous Underwater Vehicle," in Proc. MTS/IEEE OCEANS'05, Washington DC, Vol. 2, pp. 1301–1304, 2005.

[2] R. Panish, "Dynamic control capabilities and developments of the Bluefin Robotics AUV fleet," in Proc. UUST 2009, 16th International Symposium on Unmanned Untethered Submersible Technology, Lee, USA, 2009

[3] M. Caccia, "Vision-based ROV horizontal motion control: Near-seafloor experimental results," *Control Engineering Practice*, 15, pp.703-714, 2007.

[4] K. N. Leabourne, S. M. Rock, S. D. Fleischer, and R. Burton, "Station keeping of an ROV using vision technology," in Proc. MTS/IEEE OCEANS'97, Vol. 1, pp. 634–640, 1997.

[5] R. Damus, S. Desset, J. Morash, V. Polidoro, F. Hover, C. Chryssostomidis, J. Vaganay and S. Willcox, "A new paradigm for ship hull inspection using a holonomic hover-capable AUV," *Informatics in control, automation and robotics I*, Springer Netherlands, 3, pp. 195-200, 2006.

[6] W. Kazmi, P. Ridao, D. Ribas, and E. Hernández, "Dam wall detection and tracking using a mechanically scanned imaging sonar," in Proc. IEEE International Conference on Robotics and Automation, Kobe, Japan, 2009.

[7] J. Batlle, P. Ridao, R. Garcia, M. Carreras, X. Cufí, A. El-Fakdi, D. Ribas, T. Nicosevici, E. Batlle, G. Oliver, A. Ortiz and J. Antich, "URIS: Underwater Robotic Intelligent System," in *Automation for the Maritime Industries*, chapter 11, Instituto de Automática Industrial, Consejo Superior de Investigaciones Científicas, pp. 177–203, 2004.

[8] V. Creuze, B. Jouvencel, and P. Baccou, "Using sound diffraction to determine the seabed slope," in Proc. IEEE IROS 2005, Alberta, 2005.

[9] R.J. Urick, *Principles of Underwater Sound*, Peninsula Pub, 1996.

[10] X. Lurton, An introduction to Underwater Acoustics – Principles and Applications, Springer Praxis Books, 2003.

[11] V. Creuze, "Distance and Orientation Measurement of a Flat Surface by a Single Underwater Acoustic Transducer," in Proc. EUSIPCO 2011, European Signal Processing Conference, Barcelona, 2011.

[12] T.I. Fossen, *Marine Control Systems: Guidance, Navigation and Control of Ships, Rigs and Underwater Vehicles*, Marine Cybernetics AS, Trondheim, 2002.

[13] M. Caccia and G. Veruggio, "Guidance and control of a reconfigurable unmanned underwater vehicle," *Control Engineering Practice*, CEP-8(1), pp.21-37, 2000.

[14] J-J. Slotine and W. Li, *Applied Nonlinear Control*, Prentice-Hall Int, Englewood Cliffs, New Jersey, 1991.

[15] MSS. Marine Systems Simulator (2010). Viewed 01.07.2010, http://www.marinecontrol.org.